Multiscale model for ultrashort pulsed parallel laser structuring—Part III. Characterization of material properties

Thilo Barthels[a,*] **Markus Niessen**,[a] **and Christian Heinigk**[b]
[a]Fraunhofer ILT, Aachen, Germany
[b]RWTH Aachen University, Department NLD, Aachen, Germany

Abstract. In the field of microstructuring and nanostructuring ultrashort pulsed (USP) laser processing attracts increasing attention due to its ability to generate high-precision structures. A simulation of the USP process can lead to a reduced process development time and help to achieve a better geometrical quality of the manufactured microstructures. To predict the ablation shape, temperature distribution, and distortion in a USP ablation process, a detailed simulation of the physical processes during and after the laser ablation is required. Different simulation tools such as multiscale simulations are already established but still need different and accurate input parameters regarding the material properties of the workpiece to be machined. A material characterization procedure that can be used in a standardized way for different materials and processing stations needs to be developed. The procedure determines the absorption coefficient, penetration depth, and ablation threshold precisely matched to a USP machine and the material used. Based on the material characterization procedure a calibration of the used simulation has to be carried out as precisely as possible. The simulation can then be applied for a digital process development and subsequently validated with specific experiments. [DOI: 10.1117/1.OE.61.12.124108]

Keywords: ultrashort pulsed processing; material characterization procedure; ultrashort pulsed laser; micro structuring; simulation; productivity and quality; ablation.

Paper 20220187G received Feb. 24, 2022; accepted for publication Aug. 30, 2022; published online Dec. 20, 2022.

1 Introduction

Ultrashort pulsed (USP) laser technology is being used for more and more applications outside of laboratory research and has become an essential machining tool in industrial fields. This work investigates the machining of metals with USP laser radiation. The machining with USP laser radiation depends on the characteristic material properties of the workpiece to be machined and the machining process varies with different machining systems and metallic workpieces. For a more efficient design of the USP machining process, the essential material properties of stainless steel are determined within the scope of this work to subsequently calibrate an already existing simulation model of USP laser process.[1] The existing simulation model is a multiscale model for ultrashort pulsed parallel laser structuring and is presented as part I. the microscale model in the JLMN journal in 2021. Based on the existing microscale simulation model a multiscale model for ultrashort pulsed parallel laser structuring will be developed and soon presented with manuscript title: *a multiscale model for ultrashort pulsed parallel laser structuring—Part II. the macroscale model* in SPIE journal in 2022.

The common goal of the procedure to be developed here for the systematic derivation of material-specific properties for the USP processing of metals and the simulation is the digitization of feasibility studies. This will help to make the production and functionalization of components with USP laser radiation in the field of microstructuring and nanostructuring more time- and cost-efficient.

*Address all correspondence to Thilo Barthels, Thilo.Barthels@ilt.fraunhofer.de

The characterization should result in a statistically meaningful and time-efficient procedure for the characterization of USP processing systems in combination with a specific metallic material. The focus of this procedure is on the determination of laser-specific and material properties such as threshold fluence, effective penetration depth, and absorption coefficient. The determination of these three material properties relevant for USP processing has already been described in detail in various scientific works by Liu,[2] Neuenschwander et al.,[3–5] or Hermann et al.,[6] but each of these procedures describes the determination of only one of the material properties in dependence on another. In addition, different physical properties, such as multiple reflections and an angle-dependent absorption of the material, are not investigated separately during the survey of the material properties with the above-mentioned approaches. The motivation of this work is the independent and mutually isolated determination of the threshold fluence, the effective penetration depth, and the absorption coefficient in different test series by analyzing the visual impact or the shape of different ablated microstructures.

1.1 *Research Question and Agenda*

The research question is whether there is a possibility to specify a standardized material property characterization process for USP lasers. Is the approach suitable to determine the independent determination of material properties of metallic materials and are the collected material properties suitable for a calibration of a simulation?

For this purpose, the USP machining of metals is first explained by highlighting the topics of ablation model and heat accumulation. Subsequently, the state of the art will be discussed, and three recognized model approaches will be presented. Then, a procedure for the independent determination of material properties for USP machining is presented

2 Basics of USP Laser Material Processing of Metals

Short-pulse (SP) lasers are laser beam sources that emit pulsed laser light with pulse durations in the nanosecond range down to >10 ps. USP lasers are referred to pulse durations of ≤ 10 ps down to a few femtoseconds. At such low pulse durations, local sublimation of the workpiece occurs due to high energy densities during material processing. This sublimation-driven ablation is also referred to as "cold ablation" because of the absence of a melting phase and the low thermal influence on adjacent material areas. Ablation is the removal of material by vaporization on the surface of the workpiece. Figure 1 is based on a visualization approach from Eifel[7] and shows the basic factors influencing the quality of the ablation process and the productivity in terms of a production rate of microstructures per time interval, which occur during the USP laser material processing of metals.

To describe the ablation process using USP lasers, the essential material properties of the workpiece, the laser, the laser beam deflection and positioning system (in short: scanning system), the processing strategy used and the given environmental conditions (air pressure,

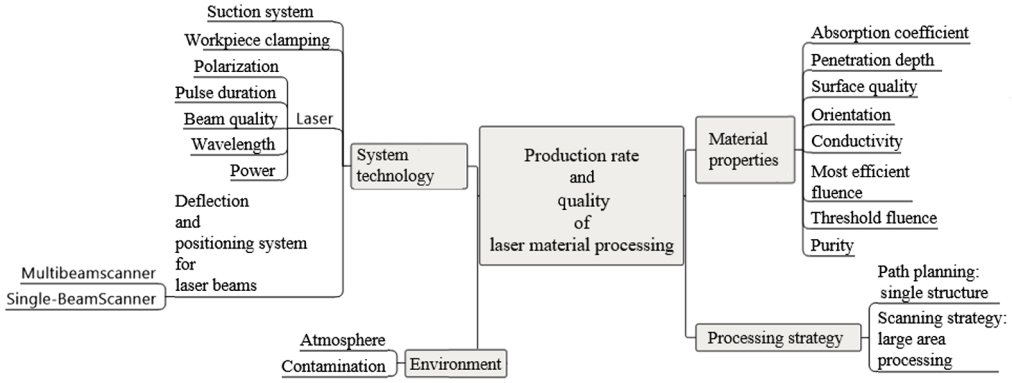

Fig. 1 Major factors influencing the material removal rate with ultrashort pulse lasers.

humidity, temperature, and so on) must be taken into account. "The large number of factors illustrates the complexity of the subject."[7] The fluence and its distribution of the laser beam are one of the most important properties for USP processing. Fluence is defined as pulse energy per area and usually given in $[\mathrm{J/cm^2}]$. For USP laser radiation, fluence is usually considered instead of intensity, which is defined as energy per time and area $[\mathrm{J/s \times cm^2}]$. When the pulse duration is in the USP range ($\leq$10 ps), during the USP ablation process the laser energy is absorbed by the electron system and transferred to the phonon (crystal lattice) system by collisions. A large part of the absorbed fluence is used for ablation. Only small portions of the fluence contribute to heating. The size of the respective portions depends on the pulse duration. But it has to be taken into consideration that the ablation behavior does not explicitly depend only on the pulse duration.[8] Due to the short time scale during a USP ablation process the time aspect and thus the intensity is rarely considered.

2.1 *Ablation Model for USP Machining of Metals*

During USP laser material processing, there is a strong short-term and local temperature increase in the material. Due to the inertia of the much heavier metal ions, the crystal lattice of the metal is heated much more slowly than the surrounding electron system. This behavior is described by the two-temperature model and was investigated in more detail by Luk'yanchuk et al.[9] Only the temperature of the crystal lattice after reaching the temperature equilibrium between the electron system and crystal lattice is decisive for the material ablation behavior.[10] Ablation only occurs when a threshold fluence is exceeded. The necessary fluence to ablate material is described according to Lambert's law

$$F_{\mathrm{abs}} = A * F_0 * \exp\left(-\frac{z}{\delta}\right), \tag{1}$$

$$F_{\mathrm{abs}} \geq F_{\mathrm{thr}}, \tag{2}$$

δ corresponds to the effective penetration depth and can correspond to an optical or diffusive penetration depth. The scientific basis for Eq. (1) has been derived by Chichkov.[11] Here, F refers to the fluence incorporated into the material and δ describes the optical penetration depth and is a material constant. Here, A refers to the absorption coefficient. By converting to z, an ablation depth per laser pulse Δz can be determined, which can be divided into two different cases:[10]

$$\Delta z = l \ln\left(\frac{F}{F_{\mathrm{thr,diff}}}\right); \quad (l \gg \delta), \tag{3}$$

$$\Delta z = \delta \ln\left(\frac{F}{F_{\mathrm{thr,opt}}}\right); \quad (\delta \gg l). \tag{4}$$

Since the respective limiting cases rarely occur in reality it is useful to introduce an effective penetration depth δ_{eff}, which can be determined from experiments. δ_{eff} is determined fluence-dependently in the experiment by the test series because the electronic properties can also change with the fluence. Here, the threshold fluence (F_{thr}) describes the tipping point from which material removal is starting. Equations (3) and (4) can be summarized with the help of δ_{eff} as follows:

$$\Delta z = \delta_{\mathrm{eff}} \ln\left(\frac{F}{F_{\mathrm{thr}}}\right). \tag{5}$$

2.2 *Heat Accumulation*

Although the heat generation when using USP laser radiation is low compared to SP laser radiation, heat accumulation effects also occur when processing with USP lasers at medium

powers >10 W.[7] Heat accumulation effects lead to a medium-term temperature increase of the workpiece and can negatively influence the quality of the ablation process. Due to the repeated impingement of laser pulses at short time intervals on the same point on the workpiece, a significant heating can occur. Strong temperature increases can lead to thermal stress, generate melt, and finally to the destruction of the workpiece.[12]

3 Material Characterization for USP Machining of Metals

Based on the ablation model presented in Sec. 2.1, various methods have been developed over time to determine material-specific properties of USP laser material processing of metals. All methods presented in Sec. 3 follow a different approach and may lead to different results. The material properties to be determined following this work are threshold fluence, effective penetration depth, and absorption coefficient. The material properties will be derived from the geometrical shapes of different structures fabricated with USP lasers.

3.1 *Determination of the Threshold Fluence*

The threshold fluence is determined for different materials taking into account the system properties. The system properties are the beam guidance and shaping, as well as the wavelength and pulse duration of the laser radiation. For pulse durations <8 ps, it has already been shown that the threshold fluence is largely independent of the pulse duration.[13] The USP laser source used in this work has a pulse duration of 900 fs. By now three different methods are known to determine the threshold fluence. B. Neuenschwander[3–5] measures the ablated volume, Liu[2] the bore radius and J. Hermann et al.[2,6] the ablation depth. For all approaches, the threshold fluence is considered a material-specific constant. The three approaches are now briefly presented.

3.2 *Determination of the Threshold Fluence According to Neuenschwander*

Neuenschwander's modeling approach for determining the threshold fluence aims to determine the threshold fluence computationally from an optimal ablation fluence. Neuenschwander represents the optimal ablation fluence as the most efficient fluence in terms of time and energy used. Neuenschwander establishes a relationship between the threshold fluence and the most efficient ablation fluence.

Figure 2 illustrates the removal behavior of stainless steel according to Neuenschwander. In Fig. 2(a), the removal rate of stainless steel in mm^3/min is plotted against the repetition rate in MHz regime for different laser powers used. Figure 2(b) shows the removal rate of stainless steel per average power in $mm^3/(min \times W)$ plotted against the pulse peak fluence as a multiple of the

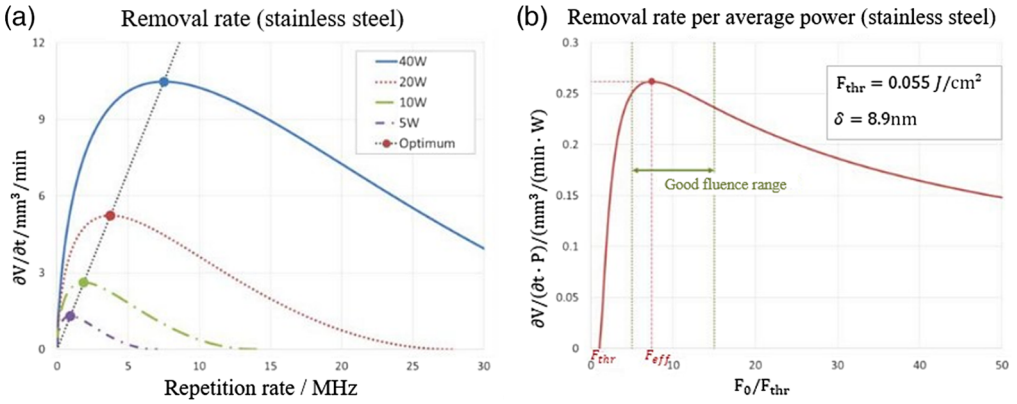

Fig. 2 (a) stainless steel removal rate for different repetition rates and (b) stainless steel removal rate per average power.[14]

threshold fluence. The removal rate per average power indicates the ratio of volume removed to the average power and process time and can thus be regarded as the ablation or removal efficiency. The fluence at the local maximum of the right graph is called the most efficient fluence (F_{eff}). The fluence at which the removal efficiency intersects the X-axis is called the threshold fluence (F_{thr}). Equation (6) represents the mathematical relationship for a Gaussian beam between F_{thr} and F_{eff}, which was determined by a working group led by Neuenschwander and confirmed experimentally[4,14]

$$F_{\text{thr}} = \frac{F_{\text{eff}}}{e^2}. \tag{6}$$

This relationship allows to determine the threshold fluence without using fluences in the order of F_{thr}. One advantage of the Neunschwander method is that it is not necessary to determine an ablation threshold in the vicinity of the threshold fluence with optical measuring systems. For this reason, different methods for determining the threshold fluence are analyzed (Sec. 4.1) A similar relationship like Eq. (6) was previously described by Raciukatis[15] with the aim of increasing the ablation efficiency.

3.3 *Determination of the Threshold Fluence According to Liu*

Liu developed a method as early as 1982 that makes it possible to determine the threshold fluence of Gaussian beam profiles. The threshold fluence is determined with knowledge of the intensity or fluence distribution and the measured radius of the ablated circular shape by using a Gaussian beam profile in the workpiece. Equation (7) shows the function of the fluence distribution as a function of the ablation radius r[2]

$$F(r) = F_0 * \exp\left(\frac{-r^2}{R^2}\right), \tag{7}$$

where F_0 denotes the pulse peak fluence and R is the radius of the focused laser beam of the laser beam. To determine the threshold fluence with the aid of Eq. (7), the workpiece surface is structured in z-direction, comparable to a percussion drilling process, and then the ablation radius r is measured. By inserting the ablation radius, the applied fluence and the previously determined diameter of the size of the focused laser beam into Eq. (7), it is possible to determine the threshold fluence mathematically.

3.4 *Determination of the Threshold Fluence According to Hermann*

Hermann establishes a linear relationship between the ablation depth per laser pulse and the natural logarithm of the fluence. With the help of this linear relationship, the threshold fluence can be determined. Figure 3 shows the averaged ablation depth over the logarithmically plotted fluence using Hermann's method.[6]

The logarithmic representation of the fluence on the x-axis results in a linear increase in the average ablation depth. By extrapolating the regression lines to the x-axis, the threshold fluence can be determined, which is in the range ≥ 0 J/cm^2 at the intersection of the regression lines with the x-axis. By transforming Eq. (8) to δ_{eff} and using the slope of the regression line by means of a gradient triangle, the effective penetration depth can be represented as follows:

$$\delta_{\text{eff}} = (\Delta z_1 - \Delta z_2) * \ln\left(\frac{F_1}{F_2}\right)^{-1}. \tag{8}$$

3.5 *Angle Dependent Absorption Coefficient*

The pulse energy deposited into the material and thus the ablation behavior is significantly dependent on the absorption coefficient. A change in the angle of incidence of the laser beam also

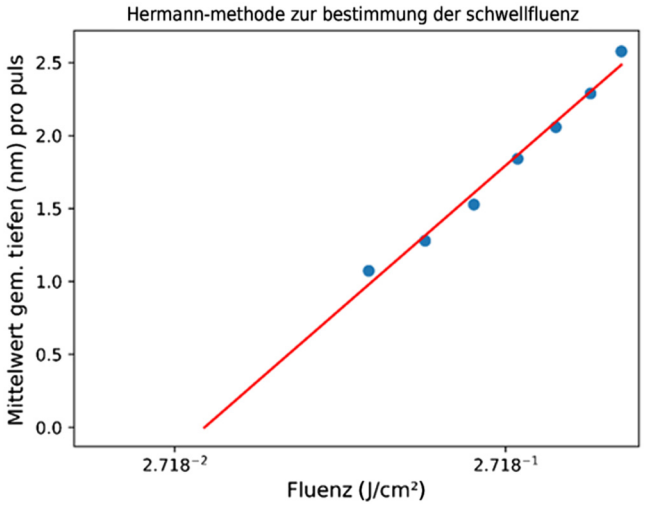

Fig. 3 Ablation depth plotted against fluence according to Hermann. Measurement data points are shown in blue, regression line in red; USP laser with 100 kHz and 900 fs; 19-μm focus diameter.

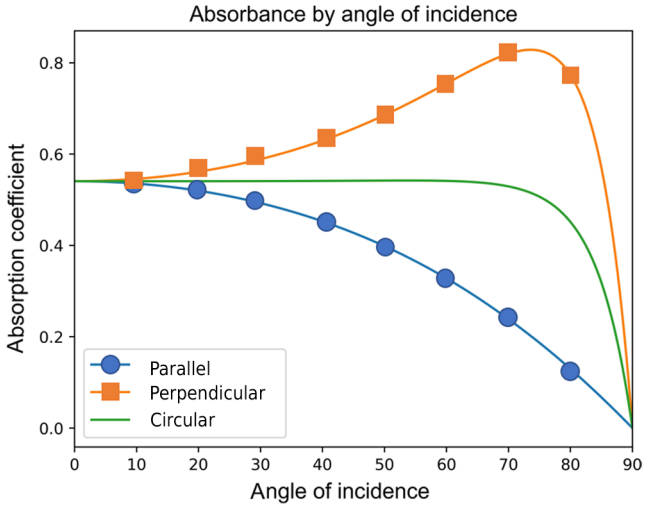

Fig. 4 Angle of incidence dependent absorption coefficient of iron for parallel, perpendicular, and circular polarization.

changes the absorption coefficient. Figure 4 shows the absorption coefficient as a function of the angle of incidence qualitatively for iron.[16]

At an angle of incidence of zero degrees, all polarization types are absorbed equally. The orange curve (squares) represents the absorption coefficient for parallel polarization as a function of the angle of incidence. The blue curve (dots) represents the absorption coefficient for perpendicular polarization as a function of the angle of incidence. The green curve describes the absorption coefficient for circular polarization and is the superposition of the two curves blue and red. Thus, during USP processing geometries with resulting tapers occur as a function of the angle of incidence of the laser radiation and the ablated depths. The degree of absorption depends on polarization and inclination angle. Even without taking multiple reflections into account, this observation explains why drilled holes are not the best choice to determine ablation thresholds. The determined ablation thresholds will depend on the geometrical shape of the drilled hole. The perpendicular polarized laser radiation is better absorbed with an increasing angle of incidence, as can be seen in Fig. 4, and the material is thus stronger ablated in the direction of the perpendicular polarization.

4 Procedure to Determine Laser and Material Characteristic Properties

A TruMicro 5280 Femto edition laser at 515 nm with an output power of 75 W, repetition rates up to 600 kHz, and a maximum pulse energy of 125 μJ was used. The laser delivers pulses at a pulse duration of 900 fs. A conventional galvo scanner is used for USP processing. In combination with an F-Theta, a focus diameter of 19 μm is generated. To precisely evaluate the ablation geometries required for the investigation, cavities with an edge length of 200×200 μm are used. The minimum ablation depth is about 3 μm and the maximum ablation depth is about 40 μm. The material used for the investigation is a 200-μm-thick stainless steel sheet made of 1.4301. Due to the pulse overlap, each location on the squared ablation area is exposed to a multiple of 100 to 1000 pulses during the ablation process. The ablation rate was calculated after measuring the ablation depth with a digital microscope (VHX-5000 from Keyence) using only the central square section of the ablated cavity. In particular, this means that the ablation depth is measured at a distance of at least 50 μm from the sides of the 200×200 μm cavity. The pulse and line overlap of 75% was chosen. The investigation was carried out for a repetition rate of 100 kHz. To robustly derive the mean depth the final depth of a cavity is measured from six identical structured geometries. This way the mean ablation depth including a standard deviation can be derived. The fluence will be investigated in a range from 0 to 25 J/cm^2.

To determine the material properties relevant for USP laser material processing four different test series are carried out. The test series are intended to analyze different physical effects in the determination process of the material properties separately from one another. The material-specific properties depend on pulse duration, wavelength, and fluence. These parameters have to be determined for the system technology used since they depend on the type of the laser system used. The series of experiments presented in this work are intended to serve as a model procedure for efficiently characterizing material properties of metallic materials. The material characterization procedure also supports the characterization of the influence of different laser beam sources using other metallic material for processing. With regard to the implementation, the required scope of experiments and the necessary statistical scope of analysis shall be derived. Figure 5 shows the classification of four fluence regions, which define the fluence ranges for four-test series (T1 to T4). The four fluence regions are chosen with respect to the characteristic behavior of the efficiency graph.

The plot illustrated in Fig. 5 represents the characteristic behavior of the ablation efficiency of a USP laser process for stainless steels.[4] On the y-axis the ablation efficiency is plotted against the pulse peak fluence as a multiple of the threshold fluence on the x-axis. Depending on the

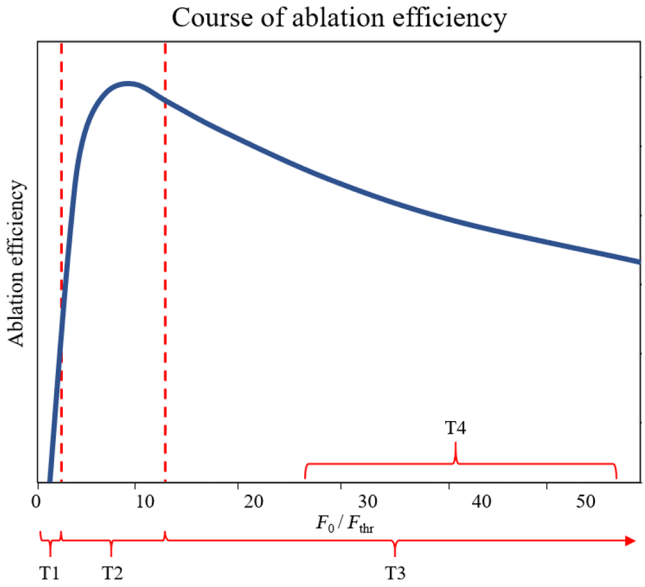

Fig. 5 Qualitative removal efficiency plotted against fluence according to Neuenschwander.

material and USP laser used the specific course of the ablation efficiency may deviate from the idealized course shown here. Based on this generally valid behavior, a division into four test series is made, which differ in their fluence range or their orientation of the polarization. In detail region T1 is used to determine the threshold fluence by using a visual approach by SEM, regions T2 and T3 are used to analyze the threshold fluence by the methods of Neuenschwander and Hermann (Secs. 3.2 and 3.4) and region T4 is used to determine the absorption properties (Sec. 3.5). For the first three test series the polarization is chosen circularly and for the fourth test series linearly to investigate the impact of p- and s-polarization. In addition to the 200×200 μm cavity approach, point ablation and line ablation have also been investigated.

In the following as the "focal area" is defined as $\pi \times {w_0}^2$ with $w_0 = 9.5$ μm. The three cross sections shown in Fig. 6 have been patterned with a fluence of 0.243 J/cm^2. The single hole has

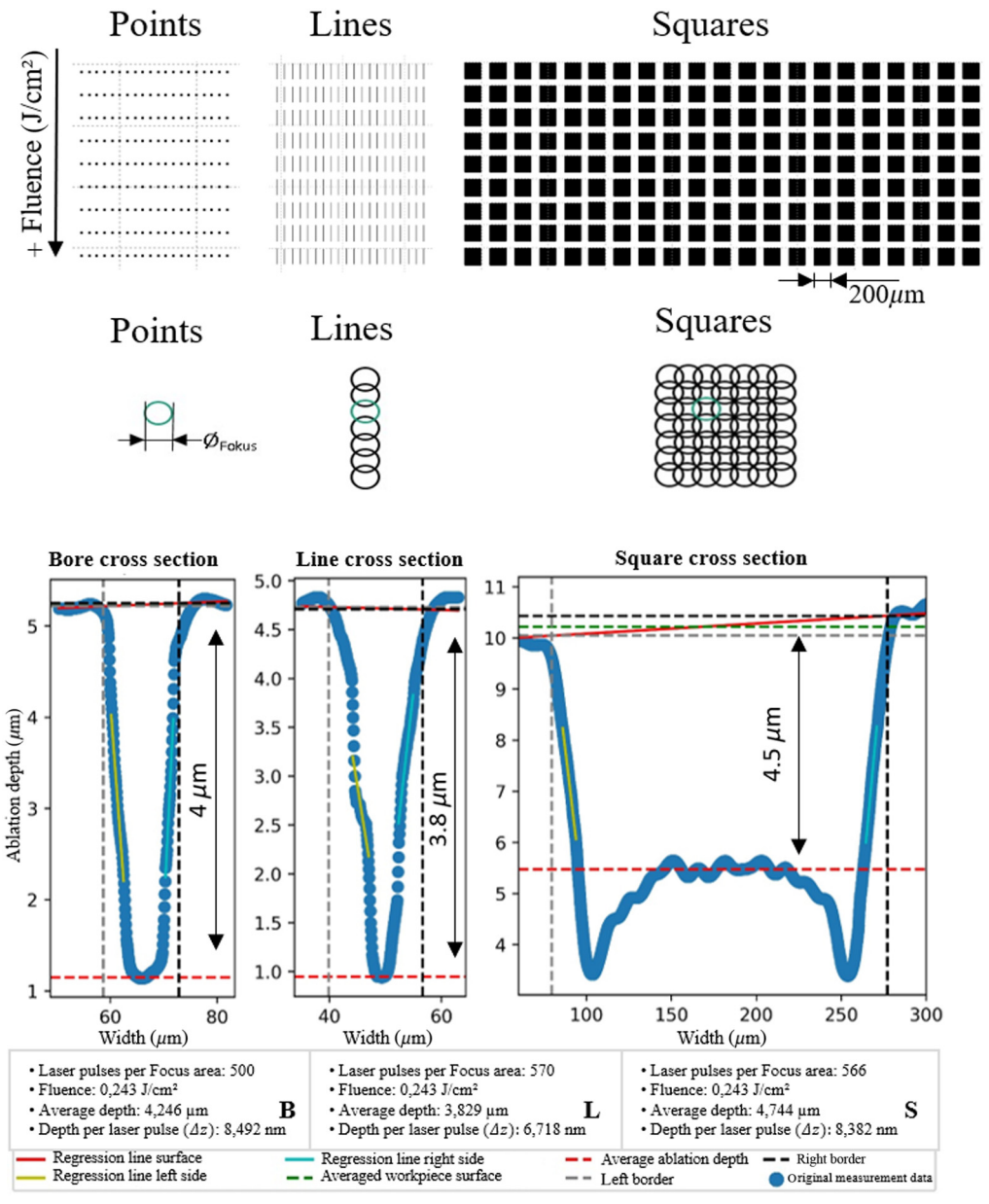

Fig. 6 Arrangement of the structured geometries on the workpiece surface by means of USP laser (top) and exemplary representation of the pulse overlap for lines and squares with focus area highlighted in green (middle). Exemplary representation of a geometry cross-section of holes, lines, and square structures (bottom).

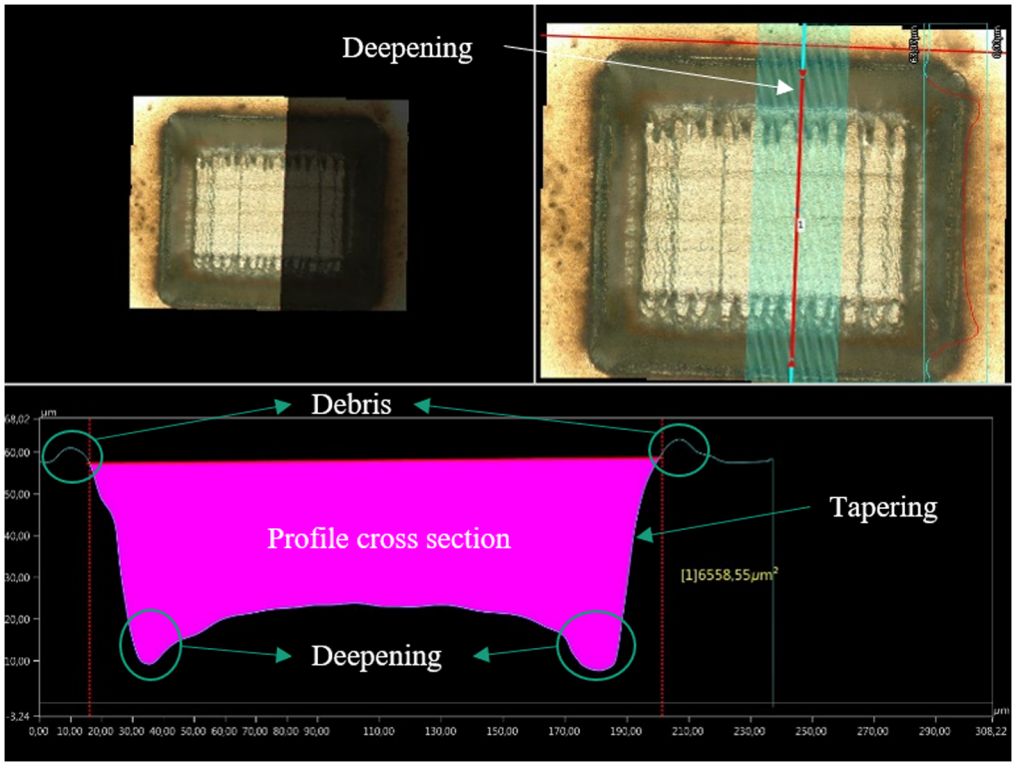

Fig. 7 Measurement result of a structured cavity square section with the VHX-5000 digital microscope.

been patterned with 500, the line geometry with 570, and the square geometry with 566 laser pulses per focal area (LpF). At the fluence and number of laser pulses per focal area used, the hole has an average ablation depth of 4.246 μm, the line of 3.829 μm, and the square of 4.744 μm. From this, the ablation depth per laser pulse Δz can be derived, which varies between the different geometries. The ablation depth for a hole and line geometry structured into the workpiece is determined using the deepest measuring point in relation to the workpiece surface (see red dashed horizontal line). To neglect the depressions at the taper (edges) of the structured workpiece, the ablated depth for a square geometry structured into the workpiece is determined using the mean plateau height (shown in Fig. 6 with a red dashed line). The depressions are neglected when calculating the average ablation depth, since influences occurring there due to the taper, such as edge reflections or different angle-dependent absorption, should not be considered. By averaging the ablation depth over the entire width of the plateau height of the square cross section, the ablation depth can be measured and reproduced more accurately in contrast to that of the bore and line cross section.

The ablation depth is measured centrally with reference to the width of the geometry in the x-direction to avoid the influence of edge reflections on the ablation depth during laser material processing. Edge reflections create depressions (deepening) at the taper of the structured workpiece surface. Please note that the scaling of the microstructure size is not identical in its width and depth in Fig. 7. The tapers and generated depressions are dark-colored, as seen in the microscope image in Fig. 7 (top). Outside the limits of the measured profile cross-section marked with red lines in Fig. 7 (bottom), convex elevations of the workpiece surface can be seen. These convex elevations are caused by recondensed material residues (debris) of the removed workpiece, which are deposited in the surroundings of the geometry and on the edges of the square structuring. To avoid the influence of the debris on the measurement result, the workpiece is cleaned with ethanol in an ultrasonic bath before measurement.

4.1 *Test Series 1: Identifying the Threshold Fluence*

The objective of the first test series (T1) is to determine the threshold fluence by a purely visual evaluation of qualitative ablation phenomena of the structured workpiece. Literature indicates that the threshold fluence of stainless steels for processing with USP lasers is in the range of 60 to 100 mJ/cm^2.[4] To determine the threshold fluence within the scope of this research the fluence is varied both above and below the known 60 to 100 mJ/cm^2. The measured average power is used to determine reasonable intervals over which the fluence can be varied in small steps. During the examination, attention is paid to when there is no ablation of the workpiece while the average power or the laser pulse energy is increased between two successive reference positions. In case there is visually recognizable ablation, the fluence at which ablation phenomena can be detected is subsequently referred to as the threshold fluence or ablation threshold.

To detect the threshold fluence, the workpiece is first machined by point geometries with multiple laser pulses. It is comparable to a percussion drilling process and Liu's approach to determine the threshold fluence (Sec. 3.3). When analyzing the experimental variation of the point geometries, it becomes apparent that a change in appearance hereinafter referred to as "modification" of the material surface can already be seen at a fluence of 25 mJ/cm^2. In addition, it can be shown that the occurrence of the modification is dependent on the number of laser pulses applied to the workpiece. Figure 8 shows an example of a digital microscope and SEM image of the variation of fluence and number of laser pulses using point structures. A test matrix for 10^2 to 10^5 applied laser pulses at different fluences at a repetition rate of 100 kHz is illustrated in Fig. 8(a). Each combination of fluence and number of laser pulses is patterned and framed five times side by side on the workpiece to highlight the homogeneity of its appearance for visual evaluation. The green line subsequently inserted in Fig. 8(a) marks the limit from which combination of fluence and number of laser pulses lead to a modification of the surface. It is obvious that with different numbers of laser pulses, a modification occurs at different fluence. This procedure, as shown in Fig. 8(a), is similar to Liu's method of elevation the threshold fluence. According to Liu's approach, a modification can apparently be mistaken for an ablation. The difference between a modification and an ablation can only be inadequately assessed by a digital microscope. Therefore, the authors assume at this point that this behavior can be attributed to the incubation effect described in literature. SEM images are able to provide a clear distinction and distinguish a first ablation result from a ripple-based modification.

The ablation threshold for a fixed combination of material and USP laser can be assumed as a constant value in J/cm^2. The present findings suggest to define a "modification threshold," which is the fluence threshold where modifications but no ablation of the material can be observed, see Fig. 8(a). When the fluence in combination with the number of applied laser pulses is sufficient to produce a visible modification of the workpiece surface, as shown in Fig. 8(b), the

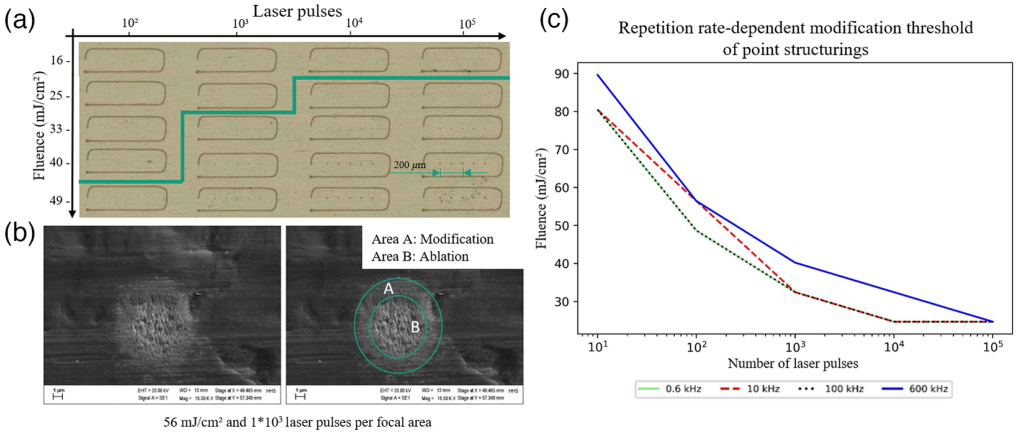

Fig. 8 Variation of fluence and laser pulse number for detection of F_{mod} at $f_{rep} = 100$ kHz (a) and point structuring of the workpiece surface at 56 mJ/cm^2 and $f_{rep} = 100$ kHz (b). Comparison of F_{mod} at different repetition rates with varying fluence and number of applied laser pulses (c).

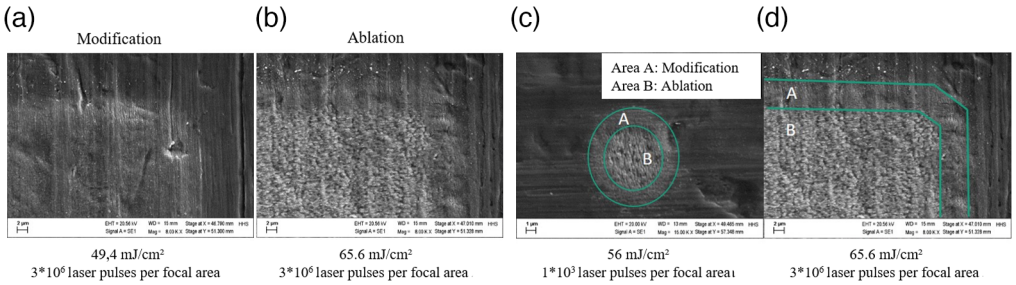

Fig. 9 Differentiation of (a) modification and (b) ablation for structuring the workpiece surface with squares at $f_{rep} = 600$ kHz and differentiation of ablation between point and square structuring of the workpiece surface for (c) $f_{rep} = 100$ kHz, and (d) $f_{rep} = 600$ kHz.

fluence leading to this first-ever modification will be referred to as the modification threshold (F_{mod}) in the rest of this paper. Figure 8(c) compares the modification thresholds of structured point geometries at different repetition rates. It can be seen that the modification threshold for point geometries is dependent on the number of laser pulses applied and not on the used repetition rate. Thus, the incubation effect is not related to the ablation threshold, but to the changing modification threshold. We observe a change in the modification threshold with the number of pulses but the ablation threshold does not change with the number of pulses. The conclusion that the modification threshold is independent of the repetition rate in a frequency range from 0.6 to 600 kHz can thus be drawn, whereby the fluctuations shown between the different repetition rates are probably due to surface contamination or material defects. At this point, however, the behavior of the modification threshold is not investigated further, since the objective is to determine the ablation threshold.

To better illustrate the difference between modification and ablation, the point geometries are replaced by squares, since a clear differentiation of the modification and ablation areas is possible due to the larger machinable area on the workpiece surface. For this purpose, 432×10^6 laser pulses were applied over the entire square with an edge length of 200 μm. To reduce the time required for the number of laser pulses applied the line spacing is set to 1 μm, the repetition rate to 600 kHz and the feed rate to 100 mm/s. This results in a pulse overlap of 90%. For square structuring, ablation first occurs at a fluence of 65.5 mJ/cm^2 in combination with 3×10^6 applied laser pulses per focal area. For USP processing of the workpiece with a fluence of 49.4 mJ/cm^2, no ablation can be demonstrated [Fig. 9(a)], which is why the ablation threshold must be in the range $49.4 < F_{thr} \leq 65.6$ mJ/cm^2. The comparison of the ablation with point and square texturing illustrates that both surface textures exhibit ripples [Figs. 9(c) and 9(d)] and that a modification region forms around the area of ablation [Figs. 9(c) and 9(d)]. The ripples seen in the square texturing are more concise than those in the point texturing and can be more clearly interpreted as ablation due to the larger textured area. Accordingly, only appearances of larger structures like square structures should be used to determine the threshold fluence. The smallest fluence leading to ablation is observed for point structuring in Fig. 9(c) at 56 mJ/cm^2, which lies in the previously determined interval [Figs. 9(a) and 9(b)] of the threshold fluence of $49.4 < F_{thr} \leq 65.6$ mJ/cm^2. It is shown that the ablation threshold is independent of the number of laser pulses.

4.2 *Test Series 2: Identifying the Most Efficient Fluence*

From literature, it is known that an efficiency maximum occurs at the pulse peak fluence (F_{eff}) which can be simply described by the product of the threshold fluence (F_{thr}) and Euler's number.[4] The experiments are varied in the interval from $3 \times F_{thr}$ to $13 \times F_{thr}$ to map the theoretical efficiency maximum at a factor of $e^2 \approx 7.39$ in the center of the fluence interval to be investigated. An important material and model property for laser material processing is the effective penetration depth of the laser radiation into the workpiece. The effective penetration depth can be determined from the values of F_{thr}, the fluence used and the ablation depth per pulse, e.g. Eq. (5).

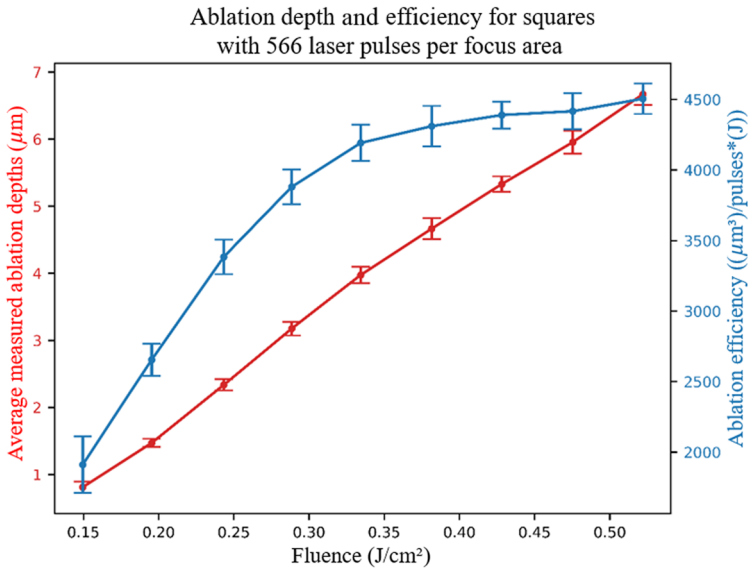

Fig. 10 Hermann and Neuenschwander graphs for different laser structured square cross section (like shown in Fig. 7) with 566 laser pulses per focal area. For the statistical purposes, six squares each with the same process parameters have been produced and measured.

In Fig. 10 the mean value of the ablation volume per pulse and pulse energy per fluence (according to Neuenschwander) and the mean value of the ablation depth per fluence are plotted for the structured squares with 566 LpF. The average ablation depth increases almost linearly with increasing fluence (red). The ablation efficiency increases with increasing fluence (blue) in the range from 0 to 0.5 J/cm^2. The efficiency maximum can be confirmed at a factor of $e^2 \times F_{\text{thr}}$ if the ablation threshold is determined visually. The effective penetration depth is calculated using the measurement points shown in Fig. 10 and the previously mentioned simulation of the USP machining process.[1] The effective penetration depth can be determined by the known ablation depth and the threshold fluence by using the simulation model[1] or the virtual volume method. The virtual volume method will be described in Sec. 4.3. Using the determined ablation threshold the simulation calculates the ablation structure for different penetration depths. By comparison with the experimental results, the penetration depth can be determined as function of the fluence. The resulting effective penetration depth in fluence range (0 to 0.5 J/cm^2) lies in the interval of 5.7 nm $< \delta_{\text{eff}} <$ 11.2 nm (Fig. 10).

4.3 *Test Series 3: Identifying the Impact of Higher Fluences*

The objective is to conduct the characterization of the material properties of stainless steel at higher fluences. Therefore, fluences from 1.76 to 24.8 J/cm^2 are investigated. It is intended to generate an understanding of the influence of comparatively high fluences for high-precision micro and nano structuring. To obtain meaningful microscopy images, the number of laser pulses used will be reduced, since measuring ablation depths >30 μm for 200 × 200 μm cavities with the VHX-5000 digital microscope can lead to under-exposure of the ablated area and thus to measurement inaccuracies. Squares are structured with an applied number of laser pulses per focal area (LpF) in an interval of 20 to 200.

The average ablation depth increases almost linearly with increasing fluence (red). In contrast, the ablation efficiency decreases exponentially with increasing fluence (blue). This suggests that the efficiency maximum is between 0.5 and 1.76 J/cm^2. The ablation for higher fluences drops nearly by a factor of 3.

In the following, the surface roughness of the manufactured cavities is investigated and presented as a function of fluence. At this point, it can also be seen that from about 12 J/cm^2 (Fig. 11), the surface roughness due to USP processing becomes worse than the initial surface

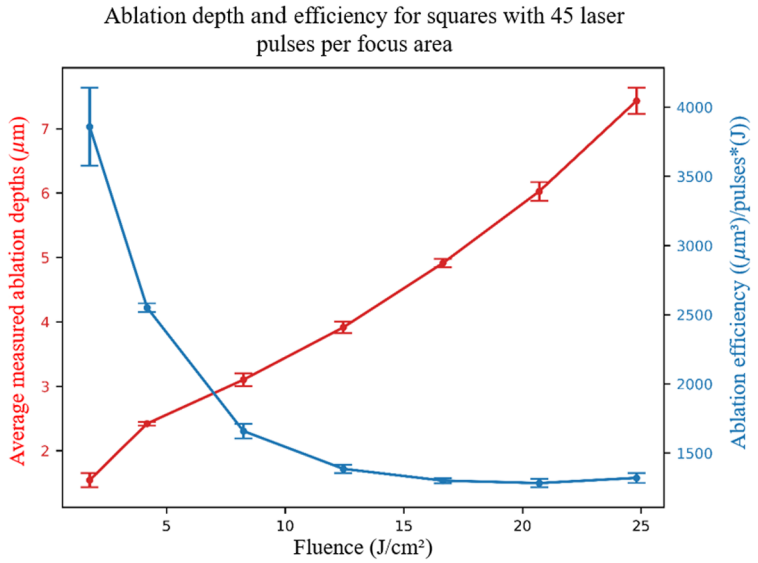

Fig. 11 Ablation depth and Neuenschwander plots for squares with 45 laser pulses per focal area at f_{rep} 100 kHz.

roughness of the stainless steel foil. Measurement point 4, shown in Fig. 12(a), is the first measurement point in Fig. 12(b) to show the noticeable trend where the determined standard deviation significantly exceeds the waviness of the original material.

Figure 12(a) shows the course of the ablated depth-averaged from six square patternings with 113 LpF over the fluence. Figure 12(b) shows that the standard deviations of these measured average ablation depths are greater than the determined line roughness of 325 nm (±160 nm) shown in Fig. 12(c). Due to the use of high fluences, temperature-related influences during machining cannot be excluded. The formation of CLPs is made possible by high fluences. CLPs are demonstrably caused by excessive thermal stress on the component during

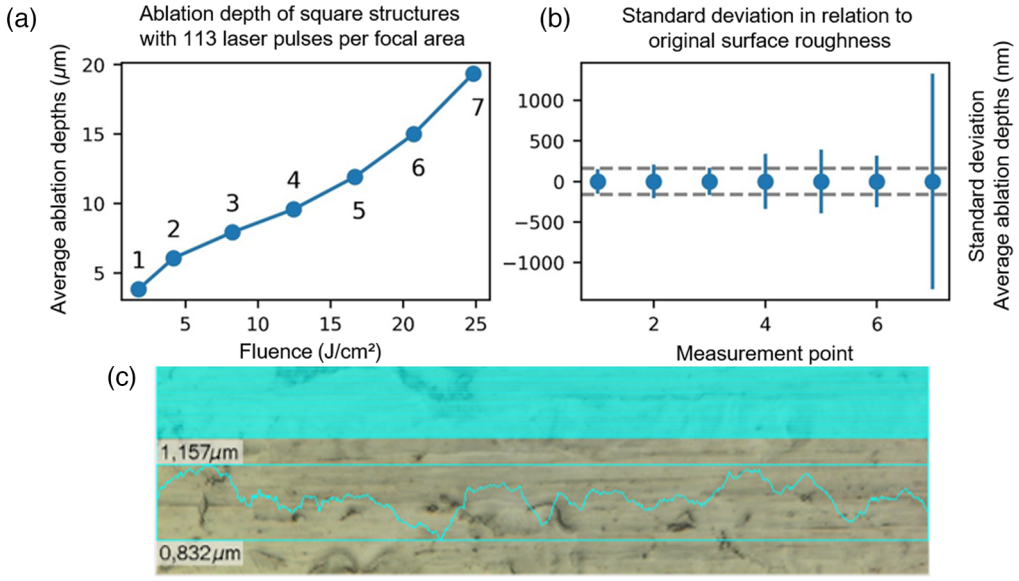

Fig. 12 (a) Mean ablation depth for 113 applied laser pulses per focal area in relation to the applied fluence. (b) Standard deviation of the ablation depth of six structured squares each with 113 applied laser pulses per focal area in relation to the line roughness of 320 nm (±160 nm). LSM measurement of the line roughness of the initial surface of the workpiece used. (c) The absolute difference is 0.325 μm and can be specified as $+/-0.160$ μm.

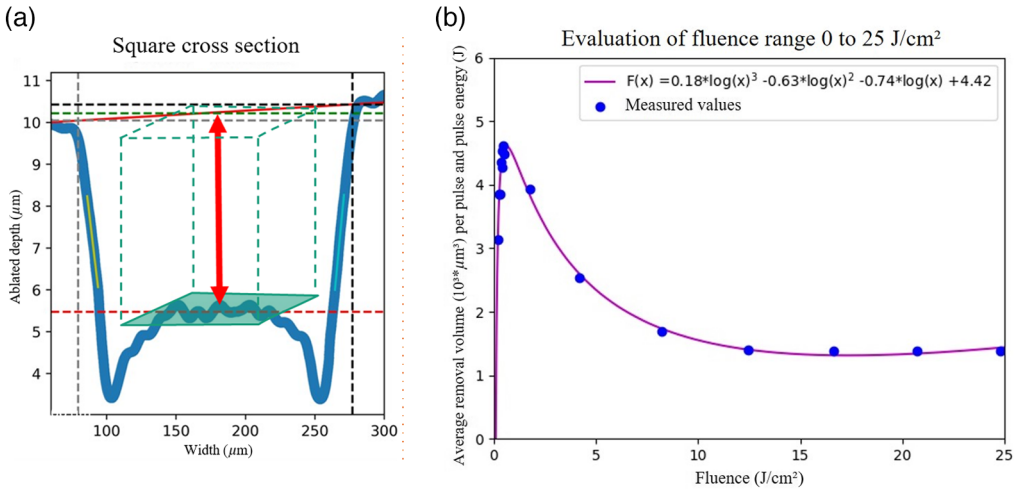

Fig. 13 Graphical approach to illustrate the procedure used to determine the ablation efficiency. (a) The approach is newly introduced and will be named as a "model of the virtual volumes" based on the presented procedure of this work. (b) Cumulative course of the ablation efficiency over the investigated fluence interval from 0 to 25 J/cm^2.

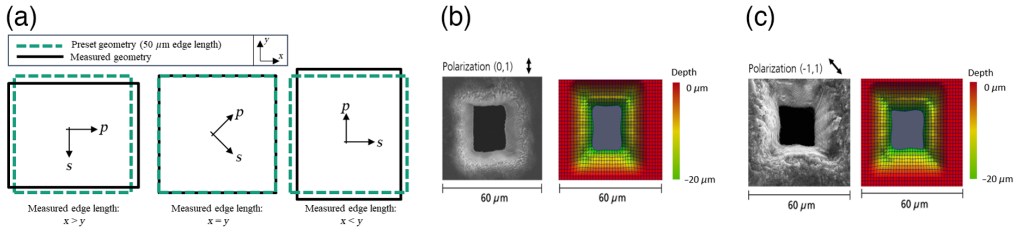

Fig. 14 (a) Influence of the angle of rotation of the $\lambda/2$-plate on the degree of ablation of the workpiece with a square structure. (b) and (c) Two different 3D model of square structure and SEM images to prove the influence of the polarization direction.

machining.[8] Due to temperature-related influences, the theoretically determined effective penetration depth may deviate from the one obtained from test series 2.

Using the ablation cross-sections of the machined squares, the effective penetration depth is determined mathematically based on the depth present at the center of the structure. For a fluence of up to 1 J/cm^2, the effective penetration depth is circa 5.7 nm $< \delta_{\text{eff}} <$ 11.2 nm and for a fluence of about 2 to 25 J/cm^2 it is 8 nm $< \delta_{\text{eff}} <$ 19.4 nm. The ablation efficiency maximum is approximately located at a fluence of 0.5 J/cm^2 [Fig. 13(b)]. The relationship between the fluence and the threshold fluence, known from the literature, is described by Eq. (6). With the determined threshold fluence of 65.6 mJ/cm^2, the ablation efficiency maximum is calculated to be 0.485 J/cm^2. This almost agrees with the result from test series 2 for a fluence of 0.5 J/cm^2. The asymptotic course of the ablation efficiency for a fluence of up to 25 J/cm^2 is shown in Fig. 13(b). The mean depth of the cross section can be used to define a virtual volume of material ablation [Fig. 13(a)]. Multiplying the mean ablation depth by a virtual two-dimensional area of any size gives a virtual ablation volume of the square structuring. The number of laser pulses applied to the total virtual ablation volume can be calculated from the feed rate, repetition rate, track spacing, and edge lengths of the virtual area under consideration. Subsequently, the required virtual ablation volume per laser pulse and pulse energy can be determined. In addition, the mean value of the virtual ablation volume and its standard deviation are computed. In this work, the collected mean values and standard deviations were composed of the measurement data of six structured squares each with processing parameters kept constant

4.4 *Test Series 4: Determination of the Absorption Coefficient*

In test series 4, the absorption coefficient of the stainless steel workpiece will be determined. The optical properties can be determined by comparison with simulation using Fresnel's equations to describe angle-dependent absorption. Here, structured squares with a specified edge length of 50 μm are machined and measured. A linearly polarized laser beam is now used to determine the absorption dependence. Figure 14(a) shows how a $\lambda/2$ plate varies the polarization by rotation and how this affects the resulting geometry of the ablated structure. Figure 14(b) and 14(c) show an SEM image and a simulated 3D model of the ablation of a square structure. On the workpiece surface, the machining strategy is identical in both cases only the linear polarization direction is changed by ∼45 deg perpendicular to the incident laser beam. In the SEM and simulation images, it can be seen that the perpendicular edges of the "square" have different lengths. Since perpendicular and parallel polarization produce different degrees of absorption at incident angles between 0 deg and 90 deg and the edges of the squares show a taper, the length and width of the squares change. They change with the set angle of rotation of the $\lambda/2$ plate which affects the orientation of the linear polarization [compare Fig. 14(a)]. The workpiece is more ablated in the direction of the *p*-polarization (compare Fig. 4). This is shown in Figs. 14(b) and 14(c) for two different orientations of the polarization.

From the aforementioned change in length and width, the angle-dependent absorption coefficient of the stainless steel workpiece can be determined for a given rotation angle of the $\lambda/2$ plate. The green dashed areas in Fig. 14(a) represent the geometries that are scanned on the workpiece surface with the scanning system. The black areas represent the geometries that are generated due to different degrees of absorption on the workpiece surface. As the angle of rotation of the $\lambda/2$ plate changes and thus the orientation of the linear polarization of the laser beam the structured geometry changes in width and length. Previously used material thickness of 200 μm proves to be unsuitable for the next step of this test series. So a workpiece with a thickness of 25 μm of the same material is used. To prevent measurement inaccuracies, several squares with the same polarization orientation are patterned through a 25 μm stainless steel foil. A rotation of the $\lambda/2$ plate by 10 deg corresponds to an optical rotation of 20 deg. To realize an optical rotation of 180 deg, the polarization orientations of the $\lambda/2$ plate are divided by steps of 10 deg per step in a range from 0 deg to 90 deg. Diffraction effects can occur during microscoping, which are manifested by blurring at the edges of the surface patterning to be measured. To avoid diffraction effects during microscoping, the square tapers on the back of the specimen are measured with incident top light. The taper angle of the square edges depends on the fluence used, therefore, two different fluences of 1.8 and 4.2 J/cm^2 will be investigated.

For the purpose of this study, taper is only of secondary importance. In the following, the length and width differences are evaluated. Figure 15 shows the length and width variation at different rotation angles of the $\lambda/2$ plate and the maximum length and width difference in each case. In Fig. 15(a), the course of the length and width change for 1.8 J/cm^2 and Fig. 15(a) for 4.2 J/cm^2. From the amplitudes of the respective plots, conclusions can be drawn about the

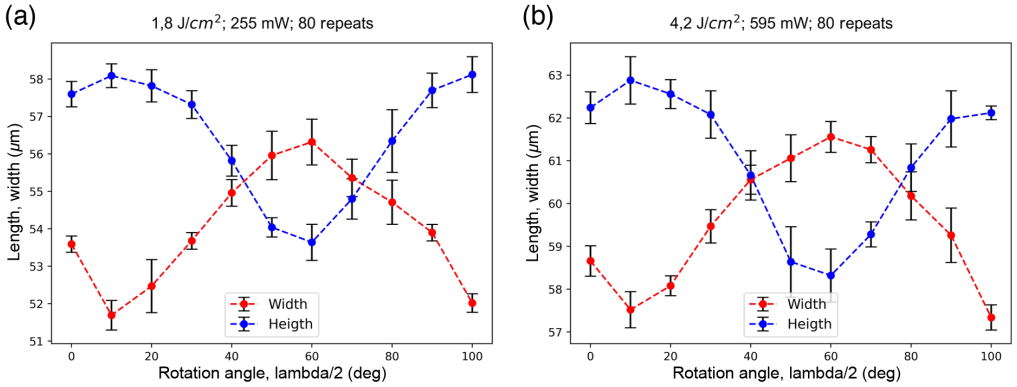

Fig. 15 Influence of the rotation angle of the $\lambda/2$-plate on the length and width of a structured square at a fluence of (a) 1.8 J/cm^2 and (b) 4.2 J/cm^2.

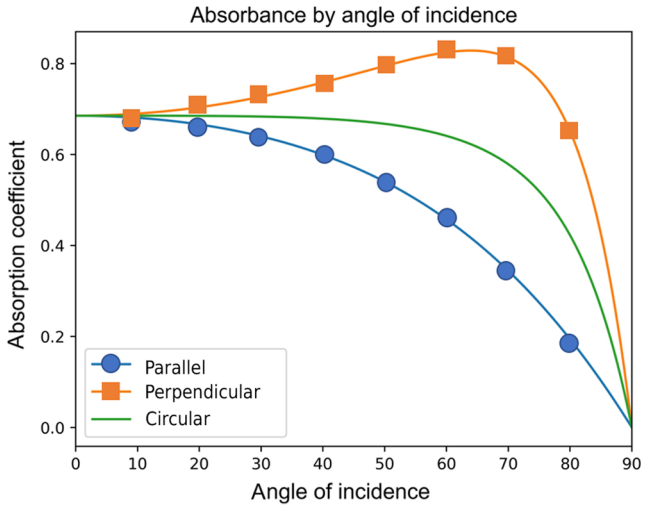

Fig. 16 Angle of incidence-dependent absorption coefficient of stainless steel.

absorption coefficient of the combination of workpiece and USP laser used. In addition, it can be observed that the squares are more strongly ablated in length (blue line) than in width (red line) by about 1.5 μm. This may be due to an elliptical raw beam or an alignment error of the laser beam. The half-length or half-width differences are defined as amplitudes. Taking into account the standard deviation for both plots the amplitudes are $\sim 2.7 \pm 0.2$ μm big.

With the amplitude of the width or length change depending on the angle of rotation of the $\lambda/2$ plate the absorption coefficient at perpendicular angle of incidence (0 deg) can be calculated to ~ 0.7. This is shown in Fig. 16. From the aforementioned change in length and width (compare Fig. 15), the angle-dependent absorption coefficient of the stainless steel workpiece can be determined for a given rotation angle of the $\lambda/2$ plate.

4.5 *Optimization of the Ultrashort Pulsed Ablation Process Using a Simulation Model*

This chapter is brief, as it is already described in more detail in the previous paper.[17] The presented procedure can be used to determine the material properties of metals such as stainless steel (material number: 1.4301) for application in USP laser surface structuring. The results from test series 1 to 4 can be used to calibrate a simulation model.[1]

Thus, a time-efficient machining process can be determined in advance by presimulation. With the help of the three material properties determined in this work (threshold fluence, effective penetration depth, and absorption coefficient), the ablation behavior of metallic workpieces during USP machining can be simulated. The machining parameters relevant for the material ablation behavior (repetition rate, feed rate, path planning, pulse energy, focus diameter, and

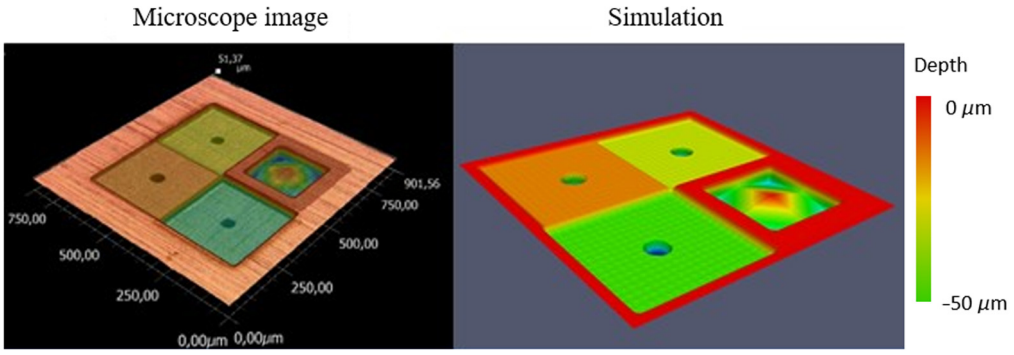

Fig. 17 Comparison of an ablation result in USP machining with a simulation.

wavelength) depend on the combination of the workpiece, machining system, and USP laser used and are transferred to the simulation. So the USP machining process can be simulated and the simulated material ablation result can be visualized. Figure 17 shows an exemplary comparison of the real USP machining process with those from the calibrated simulation. The ablation result by USP machining of the workpiece is shown in the left image of Fig. 17 by means of a microscope image with a colored height scale. The right image of Fig. 17 shows the simulated result.

5 Conclusion

The aim of this work is to develop a procedure for the efficient determination of material-specific properties of USP laser material processing. For this purpose, a division into four test series has been done. The division enables an independent determination of the three material-specific properties considered in this work: threshold fluence, effective penetration depth at low and high fluences, and absorption coefficient. It is possible to determine the threshold fluence by visual examination with the help of a scanning electron microscope. Modification and ablation threshold can be distinguished. The visible ripples of the square structure are more concise than those of the point structure and can be interpreted more clearly as ablation due to the larger structured area. The visually determined threshold fluence for point structures is 56 $\mathrm{mJ/cm^2}$ and that for quadratic structures 65.5 $\mathrm{mJ/cm^2}$. The difference between the two threshold fluence values is negligibly small, which is why the square structures are used due to their unambiguous evaluability. So the difference between ablation and modification on the workpiece surface can only be determined with the use of an SEM. If modification is misinterpreted as ablation, this can lead to incorrect conclusions about the threshold fluence. This can be an alternative explanation for the incubation effect. The threshold fluence can be determined most easily with ablated squares than with points or lines. The observed threshold fluence for ablated squares ranges from 49.4 to 65.6 $\mathrm{mJ/cm^2}$ for stainless steel (1.4301) and a USP laser with a wavelength of 515 nm and pulse duration of 900 fs. The influence of wavelength and pulse duration has already been studied and it has been shown that a USP laser with a wavelength of 515 nm and a pulse duration of approximately 800 to 1500 fs is most efficient for processing steel.[13] Since the analysis is based on discrete sequential steps with regard to the used pulse energy of the USP laser, it is recommended to use the upper interval limit of the threshold fluence range. As an estimate to the safe side by using the upper interval limit F_{thr} is 65.6 $\mathrm{mJ/cm^2}$. The visual determination of the ablation threshold is more precise than the mathematical approach via the ablation efficiency and the back calculation via the factor e^2. If the exact determination of the ablation threshold is required, it should always be determined visually with SEM images.

In summary, the following can be stated for the different methods used to determine the ablation threshold (Table 1).

Table 1 Summary of the three methods investigated for determining the ablation threshold with description and respective value of the ablation threshold.

	Method	Description	Ablation threshold value (@ 515 nm, 900 fs, 100 kHz)
1	Hermann	This method is not suitable, since the threshold fluence determined deviates too much from the other two approaches	0.088 $\mathrm{J/cm^2}$
2	Neuenschwander	This method is recommended for a quick determination of the threshold fluence. Deriving the ablation threshold based on the most efficient fluence works.	0.062 $\mathrm{J/cm^2}$
3	Visual by SEM	If a precise determination of the ablation threshold is necessary, it must be obtained by visual inspection. SEM images must then be used to clearly distinguish a modification from an ablation	0.066 $\mathrm{J/cm^2}$

The second objective is to determine the effective penetration depth for low (<1 J/cm^2) and high fluences (>1 J/cm^2). The virual volume approach is newly introduced to define the ablation efficiency and the threshold fluence without taking into consideration special processing effects like multiple reflections and angle-dependent absorption at the taper edges. By knowing the threshold fluence and calculating a virtual volume, the effective penetration depth can be determined mathematically with the depth values from the ablated cross sections. The model of the virtual volumes can be used to represent the course of the ablation efficiency more precisely, due to the fact that the impact of multiple reflections at the edges of the cavitiy is not taking into consideration. By using the virtual volume method the ablation threshold and the penetration depth can be determined.

The investigation to determine the angle-dependent absorption coefficient has been determined by varying the polarization direction when structuring the workpiece with 50×50 μm^2 geometries. The experimental output is the amplitudes of length and width of the patterned squares with varying orientation of the linear polarization. Subsequently, the degree of absorption can be determined in a simulation by means of design-of-experiment as a function of the angle of incidence. The angle-dependent absorption coefficient is important for the ablation model used in the simulation and can now be included based on the evaluation shown.

The calibration of a simulation of the USP machining process using the determined geometric data is to enable the digitization of feasibility studies. The threshold fluence can be used to calculate the effective penetration depth. Furthermore, this is not considered as a constant but as a function of the fluence. This is an important difference from the work of Liu, Neuenschwander, and Hermann. The threshold fluence together with the ablation model is used to determine the ablation depths in the simulation. Depending on the threshold fluence and the fluence used for processing, the measured and simulated ablation depths are compared iteratively. By adjusting the penetration depth used for this purpose, the comparison is made until the real and the simulated ablation depth match. The model limit has been determined to a maximum of 12 J/cm^2 while using a repetition rate of 100 kHz by the simulation in comparison with the experiments.[1]

The functional properties of the material as well as the necessary process times for process development are to be determined. The aim is to enable the series production of products using USP laser radiation in the field of micro and nano structuring as efficient as possible. One advantage of dividing the test series into four parts (Fig. 5) is that the material-specific properties can be determined independently of one another. By ablation of square structures, we achieve to avoid angle-dependent absorption and reflections, and by using different polarization directions we are able to determine the optical properties, too. Without the additional experiments with ablation structures generated with different polarization directions, the threshold fluence cannot be determined independently from the absorption properties. This means that subsequent errors during the analysis of the material properties can be avoided in future research. For all four test series, six geometries structured with the same parameters have been sufficient to obtain a mean value of the ablation depth with a sufficiently precise standard deviation. Therefore, six test structures are sufficient.

References

1. C. Heinigk et al., "A multi-scale model for ultra short pulsed parallel laser structuring — Part I. The micro-scale model," *J. Lassr Micro/Nanoeng.* **16**, 144–149 (2021).
2. L. M. Liu, "Simple technique for measurements of pulsed Gaussian-beam spot sizes," *Opt. Lett.* **7**, 196–198 (1982).
3. M. Chaja, T. Kramer, and B. Neuenschwander, "Influence of laser spot size and shape on ablation efficiency using ultrashort pulse laser system," *Procedia CIRP* **74**, 300–304 (2018).
4. B. Neuenschwander et al., "Optimization of the volume ablation rate for metals at different laser pulse-durations from ps to fs," *Proc. SPIE* **8243**, 824307 (2012).
5. B. Jaeggi et al., "Laser micromachining of metals with ultra-short pulses: factors limiting the scale-up process," *J. Laser Micro/Nanoeng.* **12**(3), 1–7 (2017).
6. J. Hermann et al., "Correlation between ablation efficiency and nanoparticle generation during the short-pulse laser ablation of metals," *Laser Phys.* **18**(4), 374–379 (2008).

7. S. Eifel, *Effizienz- und Qualitätssteigerung bei der Lasermikrobearbeitung mit UKP-Lasern durch neue optische Systemtechnik*, Apprimus-Verl., Aachen (2015).
8. J.-T. Finger, *Pulse to Pulse Interactions during USP Laser Ablation Using High Repetition Rates*, Aachen (2017).
9. B. S. Luk'yanchuk, S. I. Anisimov, and Y. Lu, "Dynamics of subpicosecond laser ablation examined by moments technique," *Proc. SPIE* **4423**, 141–152 (2001).
10. S. Nolte et al., "Ablation of metals by ultrashort laser pulses," *J. Opt. Soc. Am. B* **14**(10), 2716 (1997).
11. B. N. Chichkov, "Femtosecond, picosecond and nanosecond laser ablation of solids," *Appl. Phys. A.* **63**, 109–115 (1996).
12. J. Finger et al., "Heat input and accumulation for ultrashort pulse processing with high average power," *Adv. Opt. Technol.* **7**(3), 145–155 (2018).
13. N. Hodgson et al., "Ultrafast laser machining: process optimization and applications," *Proc. SPIE* **11673**, 1167308 (2021).
14. B. Neuenschwander et al., "Surface structuring with ultra-short laser pulses. basics, limitations and needs for high throughput," *Phys. Proc.* **56**, 1047–1058 (2014).
15. G. Raciukaitis, "Use of high repetition rate and high power lasers in microfabrication: how to keep the efficiency high?" *J. Laser Micro/Naoeng.* **4**(3), 186–191 (2009).
16. R. Poprawe, *Tailored Light 2*, Springer Berlin Heidelberg, Berlin, Heidelberg (2011).
17. T. Barthels et al., "High-precision ultrashort pulsed laser processing of metal foils using an advanced multibeam optic," *Proc. SPIE* **11267**, 112670P (2020).

Thilo Barthels studied industrial engineering with a focus on production technology at RWTH Aachen University. He completed his bachelor's and master's theses at Fraunhofer Institute for Laser Technology in cooperation with the chair of Optical Systems Technology and the chair of Laser Technology. Currently, he is in the final stages of his doctoral studies. Previous work experiences in industry include the companies 4JET, Trumpf Werkzeugmaschinen, and Pulsar Photonics.

Markus Niessen received his degree in physics from RWTH Aachen in 1991. In 1992, he became a research associate at Fraunhofer Institute for Laser Technology. In 1995, he transferred to the chair for Laser Technology, where he received his doctorate in 2005. His dissertation demonstrated the function of numerical handling of free boundary value problems in modeling. His field is the modeling and numerical simulation of dynamical processes in laser-induced material processing.

Christian Heinigk studied computational engineering science at RWTH Aachen University. In his master's thesis, he investigated mathematical methods for the efficient description of the scalar magnetic potential of a magnetic crystal. After completing his thesis, he found his way to the NLD and has been working there as a research assistant since March 2018. The main focus of his work at NLD is the modeling and simulation of laser manufacturing processes.